Communication

A Wideband Differentially Fed Dual-Polarized Antenna With Wideband Harmonic Suppression

Le-Hu Wen, Steven Gao, Qi Luo, Qingling Yang, Wei Hu, Yingzeng Yin, Xiaofei Ren, and Jian Wu

***Abstract*— A wideband differentially fed dual-polarized antenna with wideband harmonic suppression is presented. The radiating structure is composed of open slots, stair-shaped strips, and a square patch. Eight open slots are etched on the four corners of the square patch to realize symmetrical radiation and low cross-polarization for orthogonal polarizations. Stair-shaped strips are not only used to excite the open slots, but also introduce the monopole resonance. In addition, patch resonance is excited on the center square patch. For matching these different resonances, shorted microstrip lines are utilized to achieve the wide impedance bandwidth. Moreover, compact stepped impedance resonators are elaborately introduced on the top of the patch to achieve wideband harmonic suppression without any increase of the antenna footprint. The proposed antenna is designed, fabricated, and measured to verify the design method. The measured results demonstrate that the proposed antenna has the impedance bandwidth of 1.70–2.81 GHz for $S_{dd11} < -15$ dB with high isolation of 39 dB. Moreover, wideband harmonic suppression is measured from 3 to 9 GHz with the S_{dd11} higher than −2.2 dB, and the corresponding harmonic gain lower than −5.3 dBi. In addition, a stable gain of 7.2–7.9 dBi and beamwidth of 63°–71° are achieved for base station applications.**

***Index Terms*— Broadband, differentially fed antenna, harmonic suppression, stepped impedance resonator.**

I. Introduction

Because of the advantages of reduced multipath fading effect and increased communication capacity, dual-polarized antennas have been widely applied in many wireless communication systems, such as base stations, satellites, and radars. With the fast development of these communication systems [1], [2], higher requirements are put forward to guarantee the communication quality, including wide impedance bandwidth, high port isolation, low cross-polarization, and even high harmonic suppression. Recently, more and more differential devices and circuit systems are being investigated due to their high common-mode rejection and low noise level [3]. However, if the traditional single-ended antennas are utilized in the differential circuit systems, out-of-phase baluns or power dividers will be inserted, and additional insertion loss and impedance mismatching will be introduced. Therefore, it is necessary to directly research differentially fed antennas for these differential circuit systems.

Many different techniques are utilized to design differentially fed patch antennas for obtaining wideband impedance bandwidth [4]–[11]. However, due to the low profile and planar configuration, patch antennas normally face the problem of limited bandwidth and then it is difficult to meet the bandwidth requirement for base stations. Because of the wideband requirement for 2G/3G/4G base stations (1.7–2.7 GHz), dipoles are normally utilized to design wideband dual-polarized antennas [12]–[18]. These antennas can normally meet the bandwidth requirement for base stations, including the low cross-polarization, stable gain, and beamwidth. However, few of them consider the harmonic suppression of the base station antennas, which can reduce the efficiency of the power amplifiers in the transmitter, and cause serious electromagnetic interferences to the other wireless systems [19]. In addition, harmonic radiations can be received by the receiver, reducing the sensitivity of the receiver, and even congesting the receiver with strong magnitude [20]. Therefore, it is necessary to develop wideband base station antennas with harmonic suppression characteristic.

In this communication, a wideband, differentially fed dual-polarized antenna composed of open slots, monopoles, a square patch, and with wideband harmonic suppression, is presented. Eight symmetrical open slots are etched on the four corners of the center square patch to realize symmetrical and low cross-polarized radiation. Stair-shaped strips are used to excite the open slots and also radiate as the monopoles. The center square patch not only introduces the patch resonance but also leaves space for the newly incorporated function of harmonic suppression. Shorted microstrip lines are introduced for matching these three different resonances to get wide impedance bandwidth. For obtaining wideband suppression to the harmonic radiation from the antenna, compact stepped impedance resonators are elaborately introduced on the top of the patch without any increase of the footprint of the antenna. The proposed antenna was finally designed, fabricated, and measured. Both the measured and simulated results prove that the proposed antenna has the impedance bandwidth of 1.70–2.81 GHz with very high isolation of 39 dB. Moreover, compared to the traditionally designed base station antennas, wideband harmonic suppression from 3 to 9 GHz is measured with the reflection coefficient higher than −2.2 dB and related undesired harmonic gain lower than −5.3 dBi. In addition, stable antenna gain and radiation patterns are achieved for base station applications.

II. Dual-Polarized Antenna

A. Antenna Configuration

The configuration of the proposed dual-polarized antenna is shown in Fig. 1, which is composed of a square substrate printed with an antenna radiator, four coaxial cables as the antenna differential feeds, and a square copper sheet as the antenna reflector. A low-cost substrate of Rogers 4003C with the relative dielectric permittivity of 3.55 and thickness of 0.813 mm is used to fabricate the antenna. The length of the square reflector is 140 mm. Differential pairs of port 1, port 2, port 3, and port 4 are used to excite the dual-polarized antenna for ±45° polarizations. In order to facilitate the calculation of the differentially driven

Manuscript received January 30, 2019; revised April 30, 2019; accepted May 24, 2019. Date of publication June 24, 2019; date of current version September 4, 2019. This work was supported in part by the China Research Institute of Radiowave Propagation, in part by EPSRC under Grant EP/N032497/1 and Grant EP/P015840/1, and in part by the China Scholarship Council. *(Corresponding author: Le-Hu Wen.)*

L.-H. Wen, S. Gao, Q. Luo, and Q. Yang are with the School of Engineering and Digital Arts, University of Kent, Canterbury CT2 7NT, U.K. (e-mail: lw347@kent.ac.uk).

W. Hu and Y. Yin are with the National Key Laboratory of Antennas and Microwave Technology, Xidian University, Xian 710071, China.

X. Ren and J. Wu are with the Innovation and Research Center, China Research Institute of Radiowave Propagation, Qingdao 266107, China.

Color versions of one or more of the figures in this communication are available online at http://ieeexplore.ieee.org.

Digital Object Identifier 10.1109/TAP.2019.2920230

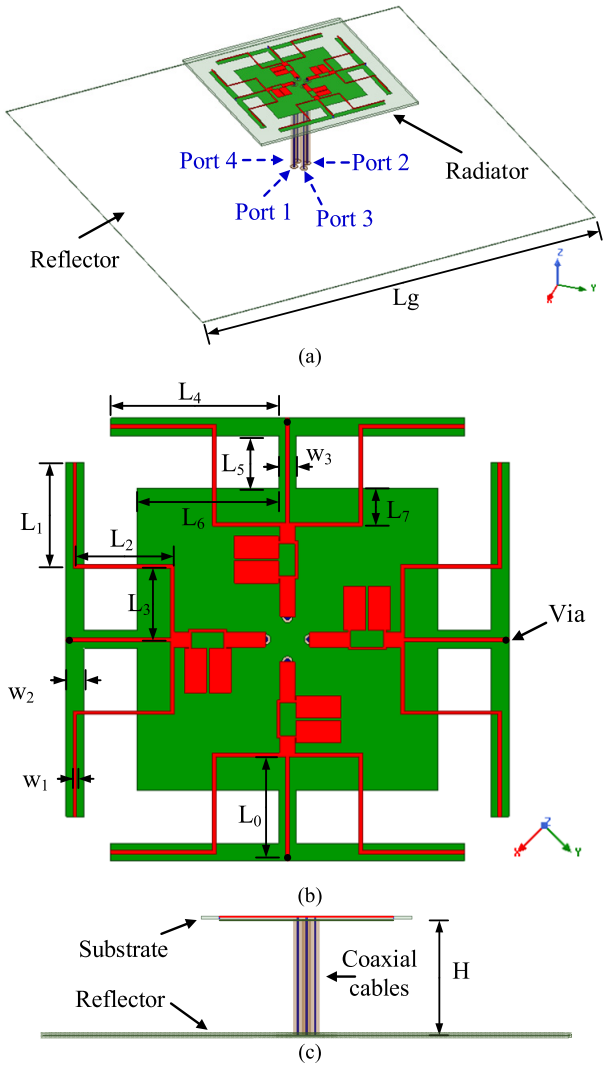

Fig. 1. Configuration of the proposed dual-polarized antenna. (a) Isometric view. (b) Top view of the antenna radiator. (c) Side view. (Detailed parameters of the proposed dual-polarized antenna: $L_g = 140$ mm, $L_0 = 11.5$ mm, $L_1 = 11.75$ mm, $L_2 = 11$ mm, $L_3 = 8.25$ mm, $L_4 = 20$ mm, $L_5 = 6$ mm, $L_6 = 16$ mm, $L_7 = 4$ mm, $w_1 = 0.4$ mm, $w_2 = 2$ mm, $w_3 = 2$ mm, and $H = 33$ mm.)

antenna, the pair of single-ended port 1 and port 2 is defined as the differential port d1, and the pair of single-ended port 3 and port 4 is defined as the differential port d2. Accordingly, the S-parameters of the differentially driven antenna can be obtained by using the single-ended four-port S-parameters [3]. In addition, because the antenna is designed for base station applications, to analyze the radiation patterns for $\pm 45^\circ$ polarizations, the xz plane, as shown in Fig. 1, is defined as the horizontal plane (H-plane), and the yz plane is defined as the vertical plane (V-plane).

Fig. 1(b) shows the details of the antenna radiator on the top and bottom layers of the substrate; the top layer is depicted in red, and the bottom layer is depicted in green. On the top layer, there are eight stair-shaped narrow strips, four narrow shorted strips, and four stepped impedance resonators, while on the bottom layer, there is a square patch connected by four T-shaped stubs. With the proposed configuration, three different resonances are developed. First, eight open slots formed by the T-shaped strips and the square patch are excited and radiate as the slot resonance. Then, the stair-shaped narrow strips are utilized to feed the open slots and also radiate as the monopoles. In addition, the square patch at the center of the bottom

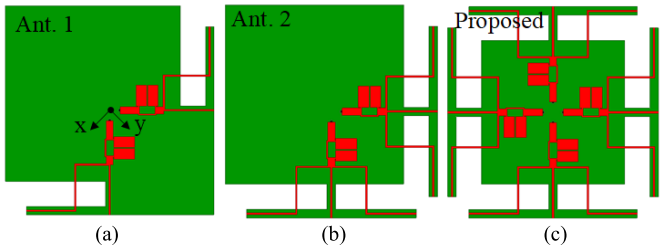

Fig. 2. Evolution process of the proposed differentially fed dual-polarized antenna. (a) Ant. 1. (b) Ant. 2. (c) Proposed antenna.

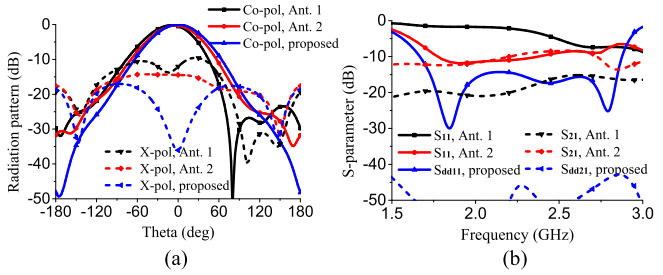

Fig. 3. Simulated results of the antennas in the evolution process. (a) Radiation patterns at 2.2 GHz in V-plane. (b) S-parameters.

layer is also resonated and radiated. For obtaining the wide impedance bandwidth, four shorted microstrip lines are introduced to match the three different resonances to feed the coaxial cables. Furthermore, to suppress the harmonic radiations of the antenna, four compact stepped impedance resonators are elaborately integrated onto the top of the patch to achieve wideband harmonic suppression without any increase of the antenna footprint. Detailed working principles of the antenna will be discussed in Sections II-B–II-E.

Fig. 1(c) shows the side view of the differentially fed antenna. Four coaxial cables are used to feed the antenna. Note that the outer conductors of the cables are soldered to the bottom square patch, while the inner conductors are soldered to the top feed microstrip lines. The height from the radiator to the reflector is 33 mm. All the simulations in this work are obtained from the 3-D electromagnetic simulation software ANSYS HFSS. The detailed optimized parameters of the antenna are listed in the caption of Fig. 1.

B. Antenna Design

It is normally difficult to realize symmetrical radiation for dual-polarization by using a single open slot. Therefore, eight symmetrical open slots are etched on the four corners of a square patch to obtain the symmetrical radiation pattern and also low cross-polarization. For an illustration of the evolution process of the presented antenna, the reference antennas are shown in Fig. 2. Ant. 1 in Fig. 2(a) has two open slots, which are etched on the two opposite corners of the square patch. Two feed lines are orthogonally arranged for dual-polarization. In Fig. 2(b), two more symmetrical open slots are added in Ant. 2. In Fig. 2(c), eight open slots are etched on the four corners of the patch to obtain the entire structural symmetry as the proposed antenna, and the antenna is fed by the differential feed ports.

Fig. 3 shows the corresponding simulated radiation patterns and the S-parameters of the reference antennas in the evolution process. Although all the reference antennas are symmetrical in the V-plane, unsymmetrical radiation patterns are still observed for Ant. 1 and Ant. 2 in the V-plane. In Fig. 3(a), Ant. 1 has the worst radiation patterns, including the unsymmetrical copolarization and the poorest cross-polarization level. After incorporating the other two symmetrical slots for Ant. 2, the symmetry of the copolarized radiation pattern is a little improved, and the cross-polarization level is reduced to some

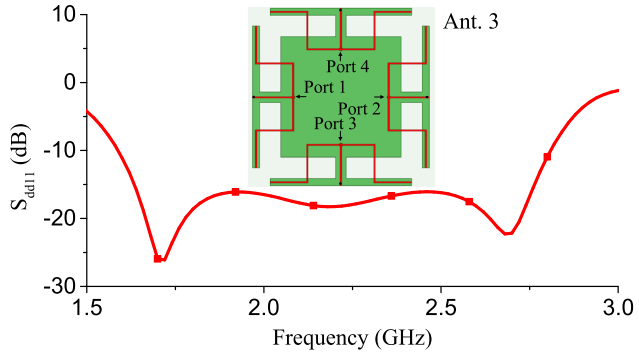

Fig. 4. Simulated S_{dd11} of the simplified reference antenna (Ant. 3).

extent. However, the radiation patterns of Ant. 1 and Ant. 2 are still worse than the proposed antenna. The main reason for these results is the strong reflections at the two input ports and the poor isolations between the two input ports for these two reference antennas, and these S-parameters are shown in Fig. 3(b). Compared to Ant. 1, worse isolation is observed for Ant. 2. This is caused by the strong coupling between the two radiating slots at the bottom right corner of the square patch. As for the radiation patterns in the H-plane, they will be more seriously affected, including the asymmetry of the copolarized radiation pattern and poor cross-polarization levels, which are caused by the asymmetry of the antenna structure in this plane. Therefore, to get symmetrical radiation patterns in both H-plane and V-plane, eight open slots are etched symmetrically on the four corners of the patch for the proposed antenna. By using the differentially fed method, orthogonal polarizations are excited with symmetrical radiation patterns and very low cross-polarization level in the broadside direction. Furthermore, the simulated S-parameters in Fig. 3(b) also show that the proposed antenna has the high port isolation (>45 dB) and the low reflection coefficient (<−15 dB) with three reflection zeroes within the bandwidth (1.68–2.8 GHz).

C. Multi-Resonance Characteristic

The proposed antenna has the multi-resonance characteristic with three different resonances, including the open slot resonance, the monopole resonance, and the patch resonance. In the configuration of the antenna, eight symmetrical open slots are introduced at the four edges of the center patch. Eight stair-shaped strips working as the monopoles are used to excite the eight open slots. The center square patch is also elaborately excited by optimizing the parameters of the antenna. For an illustration of the working principle of the three different resonances, a simplified reference antenna (Ant. 3) is investigated, and it is inset into Fig. 4. Different from the proposed antenna, four integrated stepped impedance resonators are removed from the top layer to clearly show the different resonances of the antenna. In addition, the antenna input ports are moved to the feed lines to directly reflect the input impedance of the antenna. Other configuration parameters of Ant. 3 are the same as the proposed antenna. The simulated reflection coefficient of Ant. 3 is shown in Fig. 4. Three reflection zeroes are clearly observed at 1.72, 2.18, and 2.68 GHz, and these different reflection zeroes represent three different resonances.

Fig. 5 shows the current distributions of Ant. 3 at these different resonant frequencies. In Fig. 5(a) at 2.68 GHz, strong current distributions are mainly concentrated on the surfaces of the stair-shaped monopoles, and this means the input energy is mainly radiated into the air by these monopoles. Therefore, the resonant frequency can be estimated by the length of the monopole, that is

$$f_1 \approx \frac{c}{4(L_1 + L_2 + L_3)\sqrt{\varepsilon_{r1}}}. \tag{1}$$

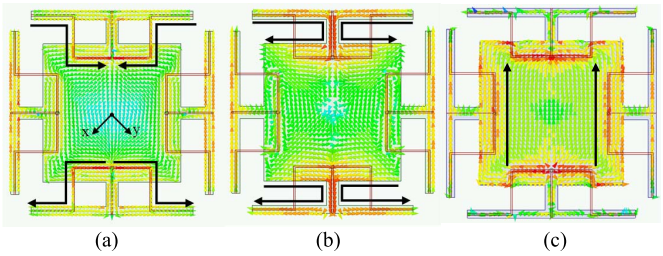

Fig. 5. Current distributions of Ant. 3 at different resonant frequencies of the reference antenna. (a) 2.68 GHz. (b) 2.18 GHz. (c) 1.72 GHz.

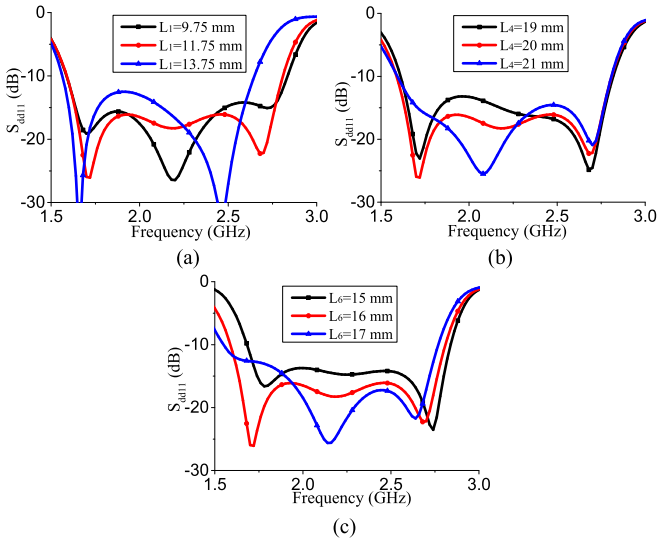

Fig. 6. Parameters study of different resonances of the reference antenna. (a) L_1. (b) L_4. (c) L_6.

In Fig. 5(b) at 2.18 GHz, strong current distributions are found on the edges of the four open slot. Slot radiation mode is excited at this frequency. So the resonance frequency can be estimated by

$$f_2 \approx \frac{c}{2(L_4 + L_5 + L_6)\sqrt{\varepsilon_{r2}}}. \tag{2}$$

In Fig. 5(c) at 1.72 GHz, strong current distributions are mainly focused on the surface of the square patch. Therefore, the patch mode is excited, and the resonance at this frequency is mainly determined by the square patch. The corresponding resonant frequency can be estimated by

$$f_3 \approx \frac{c}{2(2L_6 + w_3)\sqrt{\varepsilon_{r3}}}. \tag{3}$$

In (1)–(3), c is the light velocity in the free space, and ε_{r1}, ε_{r2}, and ε_{r3} are the effective dielectric permittivities for the monopoles, the slots, and the patch, respectively. Note that the collective current direction on the stair-shaped monopoles shown in Fig. 5(a) and four open slots shown in Fig. 5(b) is in the $\varphi = +45°$ direction, which is realized for the $+45°$ polarization. Whereas in the $\varphi = -45°$ direction, currents directions are opposite, and radiations from these opposite currents are canceled in the far-field. Therefore, a low cross-polarization level can be expected for the proposed antenna.

To illustrate the effects of the different antenna parameters on the antenna performance of the different resonances, parameters of L_1, L_4, and L_6 are studied in Fig. 6 according to (1)–(3). As shown in Fig. 6(a), when the length of the monopole L_1 becomes longer, it can be observed that the monopole resonance at the higher frequency moves to a lower frequency, whereas the other resonances almost keep unchanged. In Fig. 6(b), when the length of the open

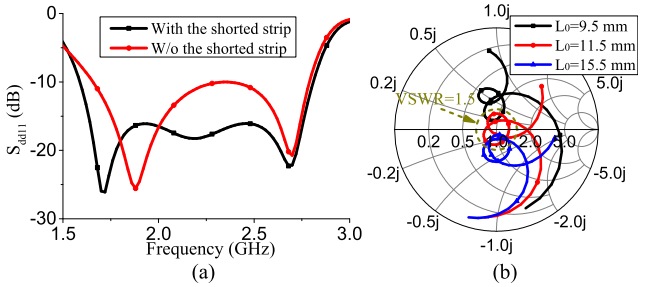

Fig. 7. Study of the effect of the shorted microstrip lines on the performance of the impedance bandwidth for Ant. 3. (a) With and without the shorted microstrip lines. (b) Variation in the length of the shorted microstrip lines.

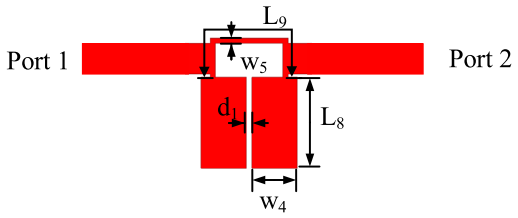

Fig. 8. Configuration of the stepped impedance resonator-based low-pass filter. (Detailed parameters: $L_8 = 5$ mm, $L_9 = 8$ mm, $w_4 = 2.5$ mm, and $d_1 = 0.3$ mm.)

slot (L_4) grows longer, the slot mode at the center frequency also moves to a lower frequency. The resonances for the monopole mode and the patch mode are almost unaffected.

When studying the parameter of L_6 for the patch mode in Fig. 6(c), the variation of the curves is a little complicated. As there is an increase in the length of L_6, the lower resonance for the patch mode moves to the lower frequency, while other resonances are affected by the change of L_6. The center resonance for the slot mode slightly shifts to the lower frequency due to the increase of the open slot length. The higher resonance for the monopole mode also shifts to the lower frequency due to the increase of the equivalent electric length for L_3, which is printed on the top of the patch. This can also be demonstrated by (1)–(3), when L_6 is changed, both f_2 and f_3 are affected. Therefore, as the change of the patch mode occurs, both the slot mode and the monopole mode will be affected.

D. Impedance Matching

For matching the three different resonances well with characteristic impedance of the differentially fed coaxial cables, shorted microstrip lines are introduced to tune the input impedance of the antenna. Fig. 7 shows the effect of the shorted microstrip lines on the impedance bandwidth of the antenna. In Fig. 7(a), when the shorted microstrip lines are removed from the antenna, it is observed that one reflection zero is disappeared on the curve with narrowed impedance bandwidth due to the mismatching between the antenna radiator and the feeding cables. Furthermore, the first reflection zero shifts to the upper frequency and the reflection coefficient at the center band is also affected and deteriorated.

To extensively investigate the variation of the length of the shorted lines, different shorted strip lengths of L_0 are studied. As shown in the Smith chart in Fig. 7(b), with the increase of the length, the inductance produced by the shorted microstrip line grows bigger. This means more inductance is shunted to the input port. Therefore, the Smith curve is moved to the inverse direction of the inductive region as the increase in the length. As shown in the Smith chart, when L_0 is selected as 11.5 mm, the widest impedance bandwidth is obtained for the antenna, and the Smith curve of Ant. 3 within the VSWR = 1.5 circle is from 1.63 to 2.77 GHz.

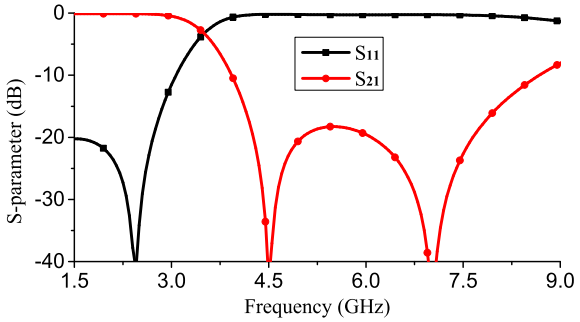

Fig. 9. Filter response of the stepped impedance resonator-based low-pass filter.

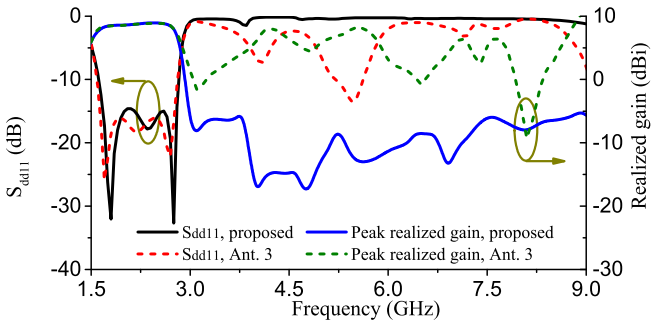

Fig. 10. Simulated S_{dd11} and peak realized gain of the proposed antenna and Ant. 3.

E. Harmonic Suppression

Thanks to the center radiating patch, compact stepped impedance resonators can be elaborately integrated on the top of the patch. Fig. 8 shows the detailed configuration of the stepped impedance resonator. The stepped impedance resonator is composed of a high-impedance microstrip line with the width of w_5 and length of L_9, and a low-impedance microstrip line with the width of w_4 and length of L_8. By using the stepped impedance resonator, an elliptic function low-pass filter can be realized with two attenuation poles [21], [22]. Fig. 9 shows the filtering response of the integrated low-pass filter. As shown in Fig. 9, the simulated reflection coefficient from 1.7 to 2.7 GHz is lower than −20 dB. Two attenuation poles are obtained at 4.5 and 7 GHz. The simulated suppression for the low-pass filter from 4.1 to 8.1 GHz is higher than 15 dB.

Fig. 10 compares the simulated S_{dd11} and peak realized gain of the proposed antenna with Ant. 3. As shown in Fig. 10, Ant. 3 has many undesired harmonic resonances and radiations. Harmonic resonances of Ant. 3 can be observed at around 4.1, 5.5, 7.15, and 7.6 GHz. Correspondingly, the peak realized gains at these frequencies are of high values, which are greater than 5 dBi. In order to reduce the antenna harmonic radiation, compact stepped impedance resonators are elaborately integrated into the proposed antenna without any increase in the antenna footprint. After the stepped impedance resonators are integrated into the antenna, the higher order harmonic resonances and radiations are greatly suppressed. Referring to the simulated results in Fig. 9, high suppression can be found at the frequencies of the two deep attenuation poles. Combining with the multi-resonance characteristic of Ant. 3, improved wideband harmonic suppression can be observed in Fig. 10. Strong reflection is achieved from 3 to 9 GHz for the antenna with the simulated $S_{dd11} > -1.46$ dB. In addition, the gain over the whole harmonic frequency band is lower than −5.1 dBi. Three-octave harmonic suppression is achieved by elaborately integrating the stepped impedance resonators into the antenna.

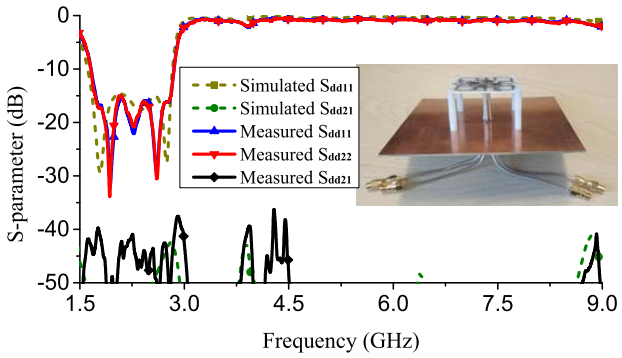

Fig. 11. Measured and simulated S-parameters of the proposed differentially fed dual-polarized antenna.

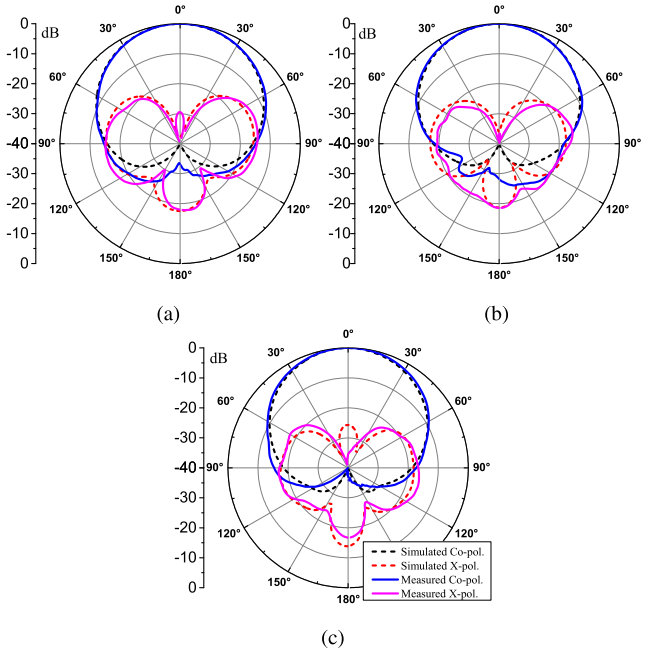

Fig. 12. Measured and simulated normalized radiation patterns of the proposed antenna in H-plane when differential port d1 is excited.

III. Results and Discussion

A. Antenna Verification

The proposed differentially fed dual-polarized antenna was fabricated and measured at the University of Kent, Canterbury, U.K. The photograph of the fabricated prototype of the antenna is inset on the right side of Fig. 11, and both the measured and simulated S-parameters of the prototype are shown for a good comparison. The measured impedance bandwidth for S_{dd11} and S_{dd22} lower than -15 dB is from 1.70 to 2.81 GHz. Owing to the symmetry of the antenna, very high isolation is measured within the whole operation band, which is higher than 39 dB. Furthermore, three-octave high harmonic suppression is achieved with the measured S_{dd11} and S_{dd22} higher than -2.2 dB from 3 to 9 GHz. Good agreement can be observed between the simulated and measured results. Small differences between the simulated and measured results are mainly caused by the fabrication and soldering errors of the feed cables.

Fig. 12 shows the measured and simulated normalized H-plane radiation patterns when differential port d1 is excited at 1.7, 2.2, and 2.7 GHz. Because of the symmetry of the antenna, only the H-plane radiation patterns are shown, and as can be seen, the measured radiation patterns agree well with the simulated radiation patterns. The measured cross-polarization level is 29 dB lower than co-polarization in the broadside direction and 23 dB lower in the $\pm$ 30° directions. The measured front to back ratio is higher than 16 dB. Fig. 13 shows the measured half-power beamwidth (HPBW) and peak realized gain of the antenna. The measured HPBW varies from 63° to 71° within the impedance bandwidth. Stable antenna gain is also achieved within the bandwidth, which varies from 7.2 to 7.9 dBi. Most importantly, wideband harmonic radiations from 3 to 9 GHz are suppressed with the maximum harmonic gain lower than -5.3 dBi.

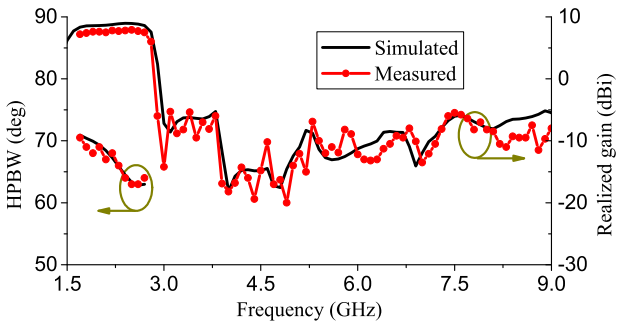

Fig. 13. Measured and simulated HPBW and peak realized gain of the proposed differentially fed dual-polarized antenna.

TABLE I
Comparison of the Reference Antennas

Ref.	Bandwidth	Height	Isolation (dB)	S_{11} of the Harmonic	Gain of the Harmonic Radiation
[12]	52% 1.7-2.9 GHz	$0.27\lambda_0$	36.3	N.G.	N.G.
[13]	48% 1.68-2.74 GHz	$0.24\lambda_0$	35	N.G.	N.G.
[14]	45% 1.7-2.75 GHz	$0.3\lambda_0$	38	N.G.	N.G.
[15]	45% 1.71-2.69 GHz	$0.4\lambda_0$	39	N.G.	N.G.
[23]	7%	0.508 mm	/	>-2.5 dB 3.5-12 GHz	N.G.
[24]	8.4%	1.57 mm	/	>-2.5 dB 5.2-13 GHz	N.G.
[25]	8.42%	0.8 mm	/	>-2.8 dB 3-10 GHz	N.G.
[26]	13.9%	1.8 mm	/	>-4.2 dB 3-9 GHz	N.G.
This work	49% 1.70-2.81 GHz	$0.25\lambda_0$	39	>-2.2 dB 3-9 GHz	<-5.3 dBi 3-9 GHz

B. Comparison

Table I compares the presented antenna with the recently published antennas. In Table I, λ_0 is the free space wavelength at the central operating frequency. Dual-polarized antennas in [12]–[15] are designed for 1.7–2.7 GHz base station applications by using crossed dipoles, dual-dipoles, or the multi-dipoles for wideband operations. Note that the antenna in [15] has the highest port isolation, but its profile is also the largest. As there is development of the wireless communication systems, more and more military and commercial wireless devices are increased in the realistic environment. If the harmonic radiations are not considered, serious interferences and congestions will be caused to affect each other's operation. To the authors' knowledge, few of these base station antennas are concerned about the harmonic radiations.

Designs in [23]–[26] are the single-polarized antennas, so there are no port isolations. For the harmonic suppression, normally only

reflection coefficients are considered, so the harmonic radiations are not provided in the references. Designs in [23] and [24] are the narrowband patch antennas. By introducing a pair of partial ring slots and an open-ended circular stub under the microstrip line [23], wideband harmonic suppression is achieved. However, additional footprint is required for these additional feed network. Designs in [25] and [26] are the slot antennas, and different shaped etched slots are employed as the defected ground structures to achieve the wideband harmonic suppression. Regarding the wideband antennas for base station applications, multiple resonances are normally employed to broaden the impedance bandwidth. Therefore, compared to the narrowband antennas in [23]–[26], more complicated harmonic radiations will be seen at the upper out-of-band, and it is more difficult to realize wideband antennas with wideband harmonic suppression. As for the presented antenna, wide impedance bandwidth of 1.70–2.81 GHz (49%) is achieved for S_{dd11} and S_{dd22} lower than -15 dB with high isolation ($>$39 dB). Moreover, wideband harmonic suppression from 3 to 9 GHz is obtained with the S_{dd11} and S_{dd22} higher than -2.2 dB. In addition, the corresponding measured harmonic radiation gain is lower than -5.3 dBi.

IV. Conclusion

This communication presents a novel wideband differentially fed dual-polarized antenna with wideband harmonic suppression for base station applications. The wide impedance bandwidth is obtained by combining different resonances from slots, monopoles, and a patch. Symmetrical radiation patterns and low cross-polarization levels are obtained by etching eight symmetrical open slots and the differential fed method. By properly changing the length of the shorted stubs, three different resonances are matched well to the feeding cables. In order to suppress the harmonic radiation of the antenna, compact stepped impedance resonators are elaborately integrated on the top of the patch with wideband harmonic suppression and without any increase of the antenna footprint. The antenna prototype was fabricated and measured for verification. The measured results demonstrated that a wide impedance bandwidth of 1.70–2.81 GHz for $S_{dd11} < -15$ dB is achieved with high port isolation of 39 dB. Moreover, wideband harmonic suppression from 3 to 9 GHz is obtained with the $S_{dd11} > -2.2$ dB and harmonic gain < -5.3 dBi. Stable gain and radiation patterns are also achieved within the bandwidth. Therefore, the proposed antenna can be a good candidate for base station applications with excellent wideband harmonic suppressions.

References

[1] S.-C. Gao, L.-W. Li, M.-S. Leong, and T.-S. Yeo, "Dual-polarized slot-coupled planar antenna with wide bandwidth," *IEEE Trans. Antennas Propag.*, vol. 51, no. 3, pp. 441–448, Mar. 2003.

[2] S. Gao, L. W. Li, M. S. Leong, and T. S. Yeo, "A broad-band dual-polarized microstrip patch antenna with aperture coupling," *IEEE Trans. Antennas Propag.*, vol. 51, no. 4, pp. 898–900, Apr. 2003.

[3] Z. Tang, J. Liu, Y.-M. Cai, J. Wang, and Y. Yin, "A wideband differentially fed dual-polarized stacked patch antenna with tuned slot excitations," *IEEE Trans. Antennas Propag.*, vol. 66, no. 4, pp. 2055–2060, Apr. 2018.

[4] K. S. Ryu and A. A. Kishk, "Wideband dual-polarized microstrip patch excited by hook shaped probes," *IEEE Trans. Antennas Propag.*, vol. 56, no. 12, pp. 3645–3649, Dec. 2008.

[5] Y.-X. Guo, K.-W. Khoo, and L. C. Ong, "Wideband dual-polarized patch antenna with broadband baluns," *IEEE Trans. Antennas Propag.*, vol. 55, no. 1, pp. 78–83, Jan. 2007.

[6] C. Deng, Y. Li, Z. Zhang, and Z. Feng, "A wideband high-isolated dual-polarized patch antenna using two different balun feedings," *IEEE Antennas Wireless Propag. Lett.*, vol. 13, pp. 1617–1619, 2014.

[7] X. Yang, L. Ge, J. Wang, and C.-Y.-D. Sim, "A differentially driven dual-polarized high-gain stacked patch antenna," *IEEE Antennas Wireless Propag. Lett.*, vol. 17, no 7, pp. 1181–1185, 2018.

[8] C. R. White and G. M. Rebeiz, "A differential dual-polarized cavity-backed microstrip patch antenna with independent frequency tuning," *IEEE Trans. Antennas Propag.*, vol. 58, no. 11, pp. 3490–3498, Nov. 2010.

[9] H. Nawaz and I. Tekin, "Dual-polarized, differential fed microstrip patch antennas with very high interport isolation for full-duplex communication," *IEEE Trans. Antennas Propag.*, vol. 65, no. 12, pp. 7355–7360, Dec. 2017.

[10] N.-W. Liu, L. Zhu, X. Zhang, and W.-W. Choi, "A wideband differential-fed dual-polarized microstrip antenna under radiation of dual improved odd-order resonant modes," *IEEE Access*, vol. 5, pp. 23672–23680, Sep. 2017.

[11] N. Liu, L. Zhu, W. Choi, and J. Zhang, "A low-profile differentially fed microstrip patch antenna with broad impedance bandwidth under triple-mode resonance," *IEEE Antennas Wireless Propag. Lett.*, vol. 17, no. 8, pp. 1478–1482, Aug. 2018.

[12] D.-L. Wen, D.-Z. Dong, and Q.-X. Chu, "A wideband differentially fed dual-polarized antenna with stable radiation pattern for base stations," *IEEE Trans. Antennas Propag.*, vol. 65, no. 5, pp. 2248–2255, May 2017.

[13] Z. Tang, J. Liu, and Y. Yin, "Enhanced cross-polarization discrimination of wideband differentially fed dual-polarized antenna via a shorting loop," *IEEE Antennas Wireless Propag. Lett.*, vol. 17, no. 8, pp. 1454–1458, Aug. 2018.

[14] Y. Cui, X. Gao, and R. Li, "A broadband differentially fed dual-polarized planar antenna," *IEEE Trans. Antennas Propag.*, vol. 65, no. 6, pp. 3231–3234, Jun. 2017.

[15] Y. Luo and Q.-X. Chu, "Oriental crown-shaped differentially fed dual-polarized multidipole antenna," *IEEE Trans. Antennas Propag.*, vol. 63, no. 1, pp. 4678–4685, Nov. 2015.

[16] L. Ge and K. M. Luk, "A magneto-electric dipole antenna with low-profile and simple structure," *IEEE Antennas Wireless Propag. Lett.*, vol. 12, pp. 140–142, 2013.

[17] Q. Xue, S. W. Liao, and J. H. Xu, "A differentially-driven dual-polarized magneto-electric dipole antenna," *IEEE Trans. Antennas Propag.*, vol. 61, no. 1, pp. 425–430, Jan. 2013.

[18] Z. L. Ma and C. H. Chan, "Waveguide-based differentially fed dual-polarized magnetoelectric dipole antennas," *IEEE Trans. Antennas Propag.*, vol. 65, no. 8, pp. 3849–3857, Aug. 2017.

[19] V. Radisic, Y. Qian, and T. Itoh, "Novel architectures for high-efficiency amplifiers for wireless applications," *IEEE Trans. Microw. Theory Techn.*, vol. 46, no. 11, pp. 1901–1909, Nov. 1998.

[20] E. Babakrpur and W. Namgoong, "A dual-path 4-phase nonuniform wideband receiver with digital MMSE harmonic rejection equalizer," *IEEE Trans. Microw. Theory Techn.*, vol. 65, no. 2, pp. 386–395, Feb. 2017.

[21] L.-H. Hsieh and K. Chang, "Compact elliptic-function low-pass filters using microstrip stepped-impedance hairpin resonators," *IEEE Trans. Microw. Theory Techn.*, vol. 51, no. 1, pp. 193–199, Jan. 2003.

[22] J.-T. Ku, M.-J. Maa, and P.-H. Lu, "A microstrip elliptic function filter with compact miniaturized hairpin resonators," *IEEE Microw. Guided Wave Lett.*, vol. 10, no. 3, pp. 94–95, Mar. 2000.

[23] S. Biswas, D. Guha, and C. Kumar, "Control of higher harmonics and their radiations in microstrip antennas using compact defected ground structures," *IEEE Trans. Antennas Propag.*, vol. 61, no. 6, pp. 3349–3353, Jun. 2013.

[24] J.-D. Zhang, L. Zhu, Q.-S. Wu, N.-W. Liu, and W. Wu, "A compact microstrip-fed patch antenna with enhanced bandwidth and harmonic suppression," *IEEE Trans. Antennas Propag.*, vol. 64, no. 12, pp. 5030–5037, Dec. 2016.

[25] C.-Y.-D. Sim, M.-H. Chang, and B.-Y. Chen, "Microstrip-fed ring slot antenna design with wideband harmonic suppression," *IEEE Trans. Antennas Propag.*, vol. 62, no. 9, pp. 4828–4832, Sep. 2014.

[26] W. Li, Y. Wang, B. You, Z. Shi, and Q. H. Liu, "Compact ring slot antenna with harmonic suppression," *IEEE Antennas Wireless Propag. Lett.*, vol. 17, no. 12, pp. 2459–2463, Dec. 2018.